PROCEEDINGS OF SPIE

SPIEDigitalLibrary.org/conference-proceedings-of-spie

Substrate-blind photonic integration based on high-index glass materials

Hongtao Lin, Lan Li, Yi Zou, Qingyang Du, Okechukwu Ogbuu, et al.

SPIE.

Substrate-Blind Photonic Integration Based on High-Index Glasses

Hongtao Lin[a], Lan Li[a], Yi Zou[a], Qingyang Du[b], Okechukwu Ogbuu[a], Charmayne Smith[c], Erick Koontz[c], J. David Musgraves[d], Kathleen Richardson[c], and Juejun Hu*[a,b]
[a]Department of Materials Science & Engineering, University of Delaware, Newark, DE 19716, USA
[b]Department of Materials Science & Engineering, Massachusetts Institute of Technology, Cambridge, MA 02139, USA
[c]College of Optics & Photonics (CREOL), University of Central Florida, Orlando, FL 32816, USA
[d]IRradiance Glass Inc., Orlando, FL 32816, USA

ABSTRACT

Conventional photonic integration technologies are inevitably substrate-dependent, as different substrate platforms stipulate vastly different device fabrication methods and processing compatibility requirements. Here we capitalize on the unique monolithic integration capacity of composition-engineered non-silicate glass materials (amorphous chalcogenides and transition metal oxides) to enable multifunctional, multi-layer photonic integration on virtually any technically important substrate platforms. We show that high-index glass film deposition and device fabrication can be performed at low temperatures (< 250 °C) without compromising their low loss characteristics, and is thus fully compatible with monolithic integration on a broad range of substrates including semiconductors, plastics, textiles, and metals. Application of the technology is highlighted through three examples: demonstration of high-performance mid-IR photonic sensors on fluoride crystals, direct fabrication of photonic structures on graphene, and 3-D photonic integration on flexible plastic substrates.

Keywords: Chalcogenide glasses, metal oxides, waveguides, resonators, integrated optical devices, sensors, graphene, flexible photonics

1. INTRODUCTION

Traditionally, photonic integration technologies are largely defined by the substrate materials the devices are built on. For example, silicon-on-insulator and silicon nitride constitute the backbone material for passive high-index-contrast photonic integration on Si (core/cladding index different $\Delta n > 0.5$), whereas waveguiding on III-V semiconductors often relies on epitaxially grown layers that exhibit comparatively low refractive index contrast (typical $\Delta n \sim 0.1$ or less). Needless to say, substrate choice also dictates the design of active optoelectronic components which are predominantly made of epitaxial single crystalline semiconductor materials. Due to the substrate-specific constraints, photonic device design rules and fabrication protocols are often non-transferrable between different substrate platforms. As a consequence, while photonic integration technologies on common substrates such as Si have been well advanced, their counterparts on unconventional substrates such as plastics, metals and functional oxides, which offer new functionalities for emerging applications including renewable energy, imaging, sensing, and display, are still in their infancy.

Our work aims to transcend the limitation by developing a platform technology that is compatible with photonic integration on different substrates. The new "substrate-blind" paradigm enables photonic integration on a vast array of unconventional substrates leveraging established knowledge base and technical know-how derived from traditional Si and III-V photonics to streamline component design iterations, improve fabrication throughput as well as yield, and thereby boost overall system performance. Further, the substrate-blind photonic integration technology also leads to unprecedented degrees of freedom in photonic design without compromising device performance. For instance, stacked multi-layer structures with complex dielectric permittivity profiles are pivotal to a number of novel devices based on slot enhancement, photonic band gap effects, or hyperbolic metamaterials. These structures conventionally present a fabrication challenge due to the need for complicated epitaxial growth, but they can be readily produced using our integration approach.

*hujuejun@mit.edu; phone 1 302 831-6878; fax 1 302 831-4545.

Nanophotonics and Micro/Nano Optics II, edited by Zhiping Zhou, Kazumi Wada, Proc. of SPIE Vol. 9277, 92770T

In this article we will start with outlining the key material requirements for substrate-blind photonic integration, which justify our choice of high-index glasses as the preferred photonic materials. Synthesis and fabrication protocols of these glasses are also briefly reviewed. We then focus on three specific examples of the substrate-blind integration strategy, all of which highlight that monolithic integration can be achieved without compromising the optical performance of devices. Lastly, the outlook of further extending our approach to multi-material and multi-functional integration is discussed.

2. THE CASE FOR HIGH-INDEX NON-SILICATE GLASSES AS A SUBSTRATE-BLIND PHOTONIC MATERIAL

Substrate-blind photonic integration stipulates several important requirements on the optical materials: 1) epitaxial-free deposition to eliminate the lattice-matching constraints; 2) tailorable optical properties commensurate with the substrate's optical characteristics: for example, material combinations with sufficient index contrast are needed for low-loss waveguiding; 3) processing compatibility with the substrate material as well as other integrated devices; 4) low processing temperature which is important not only to reducing the thermal budget but also to minimizing stress induced by coefficient of thermal expansion (CTE) mismatch – a primary cause for thin film delamination.

We hereby choose high-index non-silicate glasses (in particular, chalcogenides and Group 4 transition metal oxides such as TiO_2 and ZrO_2) as the materials to enable substrate-blind photonic integration following the aforementioned material selection criteria. Work by us as well as others have shown that deposition of these amorphous materials can be performed on different substrate materials and geometries (e.g., curved surfaces) using techniques including thermal evaporation, magnetron sputtering, pulsed laser deposition, chemical vapor deposition, or solution processing[1-13]. Most of these deposition methods can be carried out at relatively low substrate temperatures (typically below 250 °C). In addition to their monolithic integration benefit, chalcogenide glasses (ChGs) are also known for their almost infinite capacity for composition alloying and property tuning: for example, their refractive indices can be continuously tuned from 2.0 to 3.5 by composition engineering. Their optical transparency window may be tuned as well from visible up to long-wave infrared. Similarly, amorphous TiO_2-ZrO_2 alloy have continuously tunable index from 2.0 to 2.4. The composition design agility thus allows precise tailoring of the glasses' properties to meet the specific integration needs.

3. MATERIAL SYNTHESIS AND DEVICE FABRICATION PROTOCOLS

In our experiments, the ChG thin films were deposited from bulk glass samples by thermal evaporation or spin coating from organic amine solutions[14]. During thermal evaporation, the substrate is constantly held near room temperature. Spin coated films, on the other hand, have to undergo an annealing treatment to facilitate residual solvent removal, which typically consists of baking the sample at 140 °C in vacuum for up to 8 hours. TiO_2 films were synthesized using a sol-gel method and deposited via spin coating or dip coating. Subsequent annealing at 250 °C for 20 minutes stabilizes the film micro-structure.

Subsequent device fabrication on ChG films were performed using lift-off[15] or thermal nanoimprint[16-18]. Both methods are capable of generating sub-micron single-mode optical waveguides. TiO_2 devices were patterned using standard UV lithography followed by plasma etching. Device patterns were transferred to the TiO_2 layer using Inductively Coupled Plasma (ICP) RIE in mixed CF_4, Ar and O_2 gases (volume ratio 16:4:3, total pressure 2 Pa) and at a microwave power of 500 W with 150 V bias. Three types of devices were fabricated to demonstrate our substrate-blind integration approach: 1) mid-IR micro-disk resonators and multi-layer slot resonators on IR-transparent CaF_2 substrates; 2) flexible photonic devices on plastic substrates; and 3) monolithic photonic structure fabrication on graphene.

4. MID-IR RESONATOR SENSORS ON FLUORIDE CRYSTALS

Here we leverage the monolithic integration capability of ChGs to demonstrate a high-performance, versatile glass-on-CaF_2 platform for mid-IR integrated photonics. The glass-on-CaF_2 system can potentially operate over a wide wavelength range from 600 nm to 7.5 μm, only limited by the phonon absorption onset in the CaF_2 substrate at 7.5 μm.

The ChG microdisk resonators were fabricated using a negative-resist-based lift-off process adapted to fabrication on CaF_2 substrates. Lithographic patterning was performed using standard i-line UV exposure on a mask aligner. $Ge_{23}Sb_7S_{70}$ was chosen as the glass composition for this application given its superior thermal and chemical stability compared to its classical As-based counterparts (As_2S_3 or As_2Se_3). Fig. 1a shows the SEM cross-section of a $Ge_{23}Sb_7S_{70}$ glass waveguide. The small cross-section waveguide supports a single quasi-TE mode shown in Fig. 1b. A pulley

coupler design was used to increase coupling strength between the feeding waveguide and the microdisk resonator as shown in Fig. 1d[15].

Mid-IR optical transmission characteristics of the devices were measured using a fiber end-fire coupling method around 5.2 μm wavelength. Details of measurement setup can be found elsewhere[19]. Fig. 2a plots the transmission spectrum measured from a 100-μm-radius micro-disk resonator. Free spectral range (FSR) of the resonator measured from the spectrum is 20.52 nm. The corresponding group index of the whispering gallery resonant mode is 2.1, which agrees well with our finite-element modal simulations. Notably, doublet peaks were consistently observed on our resonator devices, clearly indicating the lift of degeneracy between two standing wave modes caused by roughness backscattering.

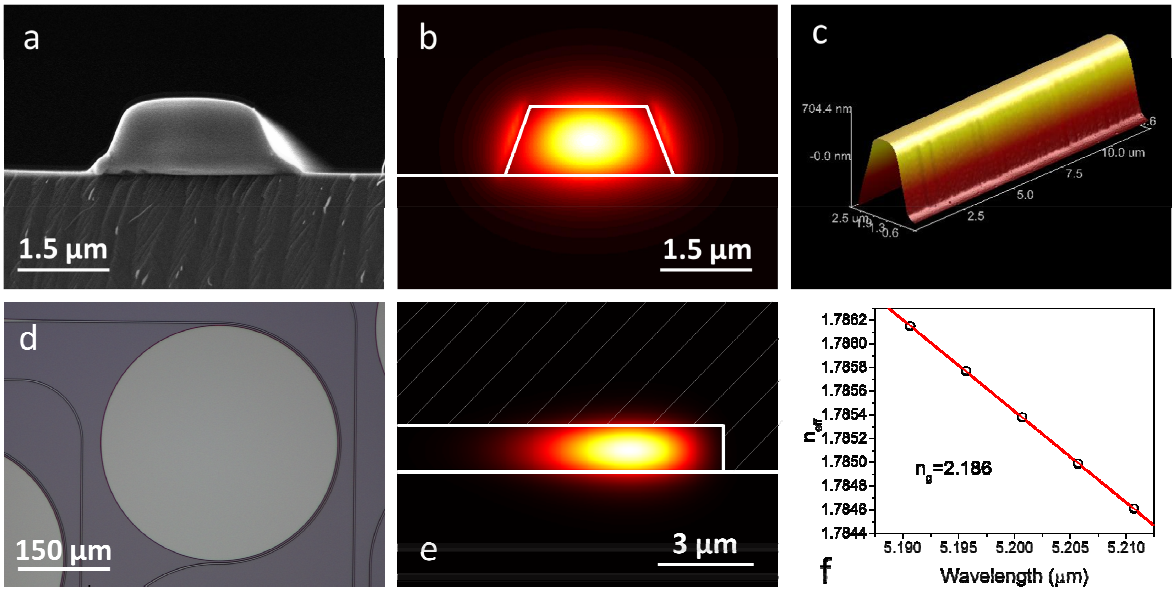

Figure 1. (a) SEM cross-section image and (b) mode profile of a 3 μm by 1.3 μm $Ge_{23}Sb_7S_{70}$ on CaF_2 single mode waveguide at 5.2 μm wavelength; (d) microscope image of 100 μm radius pulley coupled disk resonators inset shows the well-defined gap between the bus waveguide and resonator; (e) profile of first order whispery gallery mode (WGM) of a 100 μm disk resonator; (f) simulated effective index dispersion of the WGM.

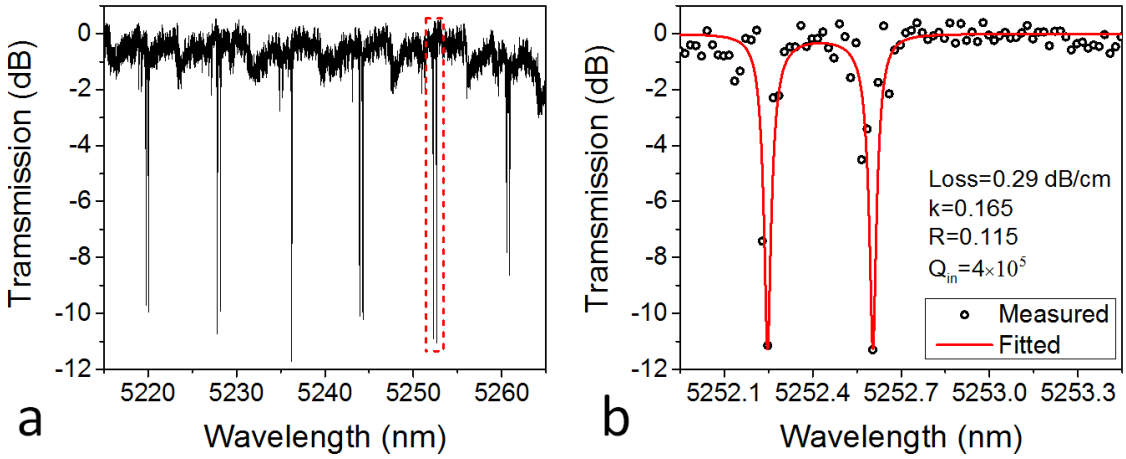

Figure 2. (a) Mid-IR transmission spectrum of a micro-disk resonator; (b) the same spectrum near an optical resonance peak (red box in a); measured data were fitted by coupled mode theory, and the intrinsic quality factor is about 4×10^5.

Transmission spectra of the resonator devices were fitting using the couple mode theory which also takes into account coupling between clockwise and counter-clockwise whispering gallery modes due to backscattering. The Q-factors were

extracted by fitting of the transmission spectra. The device exhibits an intrinsic quality factor of 4×10^5. To the best of our knowledge, this represents the highest Q value ever reported in mid-IR on-chip resonators.

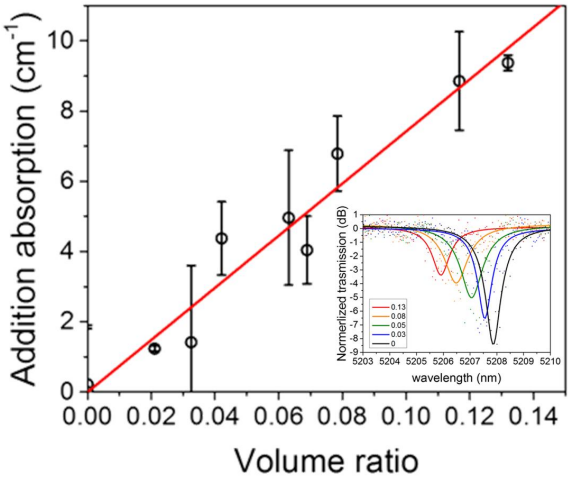

Figure 3. Optical absorption induced by ethanol as functions of ethanol volume ratio measured by the resonator sensor. The inset plots the mid-IR transmission spectrum of a 200 μm radius disk resonator in ethanol/cyclohexane solutions of different volume ratios.

We further demonstrated on-chip mid-IR cavity enhanced chemical sensing capitalizing on the resonantly enhanced light-matter interactions in the resonator. In the experiment, cyclohexane solutions containing different concentrations of ethanol was pipetted onto the resonator chip and the resonator transmission spectra were monitored *in-situ*. Cyclohexane was chosen as the solvent as it only exhibit a weak, flat absorption background in the wavelength range of interest (5.1 – 5.3 μm). On the other hand, ethanol has a weak (relative to its main IR absorption band at 3.9 μm which has an absorption coefficient of 2900 cm^{-1}) absorption peak centered around 5.2 μm wavelength. Fig. 3 inset shows the resonator transmission spectra as the device was immersed in cyclohexane solutions. The progressive decrease of extinction ratio with increasing ethanol concentration is a consequence of excess optical absorption induced by ethanol. Addition optical absorption induced by ethanol was obtained by subtracting the waveguide loss in pure cyclohexane from the total propagation loss when ethanol was present, and normalized by the modal confinement factor in the sensing region shown as the shaded area in Fig. 1e. The confinement factor is 0.10 based on our finite differential modal simulation for the waveguide we used in the experiments. Concentration-dependent optical absorption of ethanol at 5.2 μm wavelength was plotted in Fib. 3. The absorption coefficient of ethanol in cyclohexane can be obtained by a linear fit of the plot to be $\alpha_{ethanol} = (74 \pm 3.4)$ cm^{-1}, which agrees well with measurement result ($\alpha_{ethanol} = 78$ cm^{-1}) obtained on a bench-top Fourier Transform Infrared (FTIR) spectrophotometer.

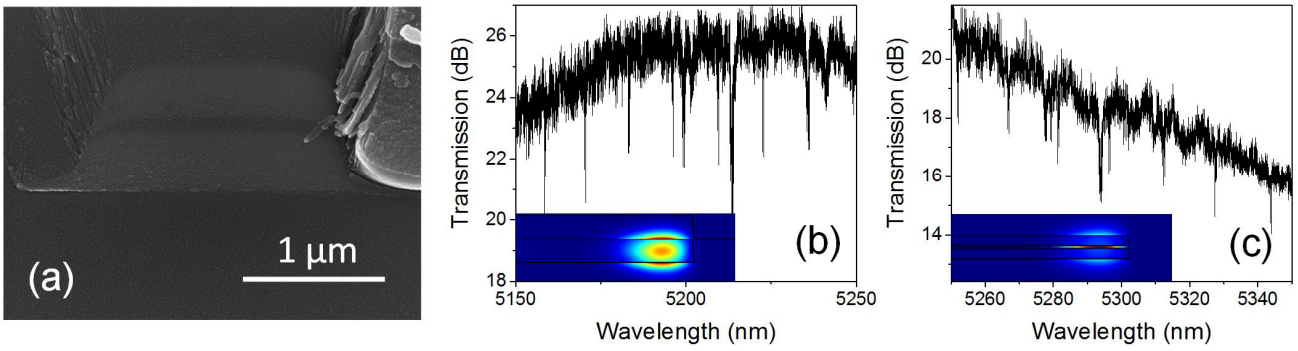

Figure 4. (a) SEM micrograph of a mid-IR horizontal slot waveguide end facet; (b) transmission spectra of a GAST glass resonator without slot; (c) transmission spectra of a slot resonator.

The monolithic integration capacity of glasses can also be readily exploited to fabricate complex multi-layer structures. One such example is horizontal slot waveguides[20], which have been shown to be an effective device platform for broadband dispersion engineering[21]. We fabricated slot waveguides and resonators by sequential deposition of

GeAsSeTe (GAST) glass (n = 3.2) and GeSbS glass (n = 2.0) layers. Fig. 4a presents an SEM cross-section of a horizontal slot glass waveguide, clearly showing the GeSbS layer sandwiched between two GAST strips. Transmission measurements were performed on microdisk resonators without and with the slot layer and their transmission spectra are plotted in Fig. 4b and 4c, respectively. The loaded Q-factor of the slot resonator is 40,000, slightly lower than that of GAST resonators without the slot (Q = 80,000).

5. FLEXIBLE PHOTONIC DEVICES ON PLASTIC SUBSTRATES

Besides their entrenched roles in information technology, photonics is increasingly penetrating into other emerging arenas including biotechnology and healthcare. Integrated photonic devices are ideally suited for *in-vitro* and *in-vivo* sensing, diagnostics, therapeutics, and stimulation given their small form factor, low power consumption, mechanical robustness, large multiplexing capacity, as well as strong light-molecule interactions enabled by tight optical confinement. Nevertheless, conventional photonic integration is pre-dominantly carried out on rigid semiconductor substrates, and their mechanical stiffness makes the devices inherently incompatible with soft biological tissues. Conformal sensor integration on skins serves as another example where mechanical flexibility becomes indispensable.

Here we demonstrate monolithic photonic integration on plastic substrates using high-refractive-index ChGs[22, 23] and TiO_2. As stated previously, both materials can be deposited directly on plastic substrates at reduced temperature. In particular, TiO_2 is also uniquely poised for flexible photonic integration given its known biocompatibility. Fig. 5 schematically illustrate the device fabrication process flow.

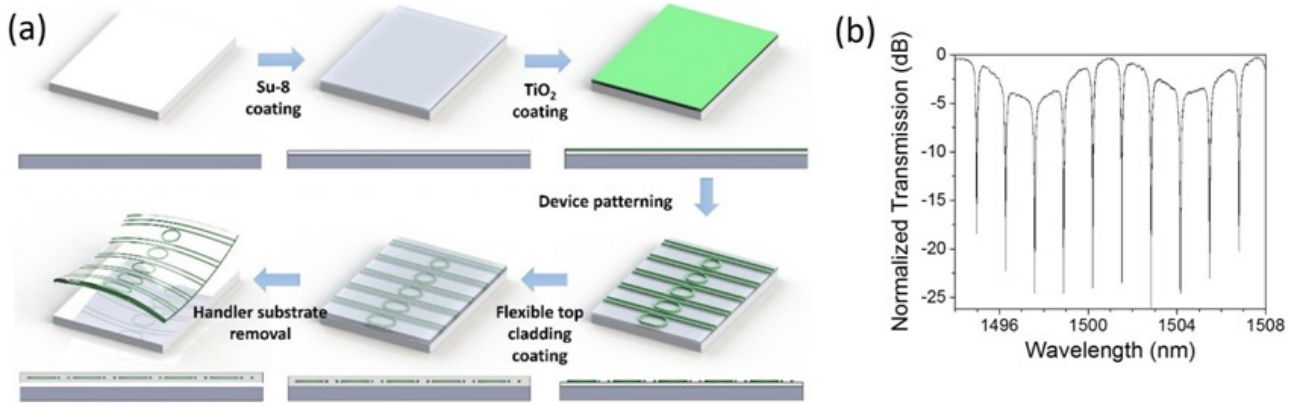

Figure 5. (a) Schematic illustration of the flexible TiO_2 device fabrication process; (b) normalized optical transmission spectra of a TiO_2 racetrack ring resonator.

The flexible waveguides and resonators were mounted on motion stages and characterized using the fiber end fire coupling method *in-situ* both in a "flat", undeformed state and when subjected to bending. For ChG micro-disk resonators, we measured an average intrinsic Q-factor of 2.7×10^5 and a highest Q-factor up to 4.6×10^5, which represents the highest Q-factor reported in flexible photonic devices[22]. Fig. 5b present a typical transmission spectrum of a flexible TiO_2 resonator, and an intrinsic Q-factor of 2×10^4 is fitted from the spectrum. The loss number and Q-factor is comparable to previously reported values in sol-gel devices: Park *et al.* measured a propagation loss of 15 dB/cm and an intrinsic Q-factor of 2×10^4 in TiO_2 WGM resonators near 1550 nm wavelength[24].

A novel multi-neutral-axis design is implemented to render the structure highly mechanically flexible[22, 23]. The design involves sandwiching a low elastic modulus layer between two stiff layers. The soft layer serves as an effective strain relieving agent which reduces the strain in on the multi-layer stack surface. Our flexible photonic devices fabricated following the design recipe can sustain repeated bending of the devices down to sub-millimeter bending radii with minimal optical performance degradation. As an example, Fig. 6a plots the insertion loss of a flexible $Ge_{23}Sb_7S_{70}$ ChG waveguide before and after up to 5,000 bending cycles: the same waveguide was used throughout the measurement to ensure consistent facet quality. The intensity fluctuations were partially attributed to excitation of higher order modes at the 2 μm wide input/output waveguide taper sections. The changes of waveguide propagation loss deduced from the measurement were plotted in Fig. 6b. The results indicate a minor (0.5 ± 0.3) dB/cm waveguide loss increase after 5,000 cycles at a frequency of 1.5 Hz. The same fatigue tests were performed on $Ge_{23}Sb_7S_{70}$ micro-disk resonators. After 5,000 bending cycles, we observed a 23% decrease of the device intrinsic Q-factor. We inspected the flexible chip under

optical microscope (up to 50x magnification) before and after 5,000 bending cycles and no micro-cracks were observed across the chip. Therefore, we conclude that the minor loss increase (~ 0.5 dB/cm) likely stems from layer delamination or sub-micron cracks that cannot be resolved with an optical microscope. To the best of our knowledge, our study represents the first report of fatigue analysis on flexible micro-electronic or micro-photonic devices that can sustain sub-millimeter bending.

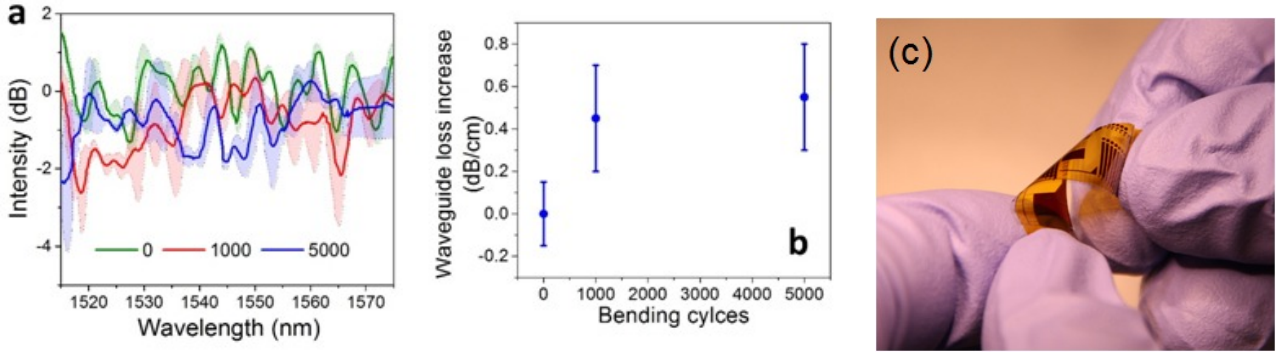

Figure 6. (a) Normalized optical transmission spectra of a flexible waveguide after multiple bending cycles at 0.8 mm bending radius. The shaded regions denote the measurement error bar, which was defined as the standard deviation of optical transmittance collected in multiple transmission measurements; (b) spectrum-averaged (1510-1580 nm wavelengths) waveguide propagation loss change due to repeated bending cycles; (c) photo of a flexible ChG photonic chip.

6. MONOLITHIC PHOTONIC DEVICE FABRICATION ON GRAPHENE

Our substrate-blind integration approach is also applicable to photonic integration on emerging 2-D materials such as graphene. Crystalline waveguide materials such as Si cannot be epitaxially grown on graphene. Further, since clean graphene is chemically inert, uniform dielectric layer deposition has been a challenge especially for atomic layer deposition[25]. Therefore, the traditional solution involves transferring graphene layers on top of fabricated photonic circuits. This approach is however limited in its integration capacity and cannot be used to create complex 3-D photonic structures involving multiple graphene or waveguiding layers. Here we show that ChGs can be directly deposited on CVD grown graphene on its growth substrate as well as after transfer to foreign substrates.

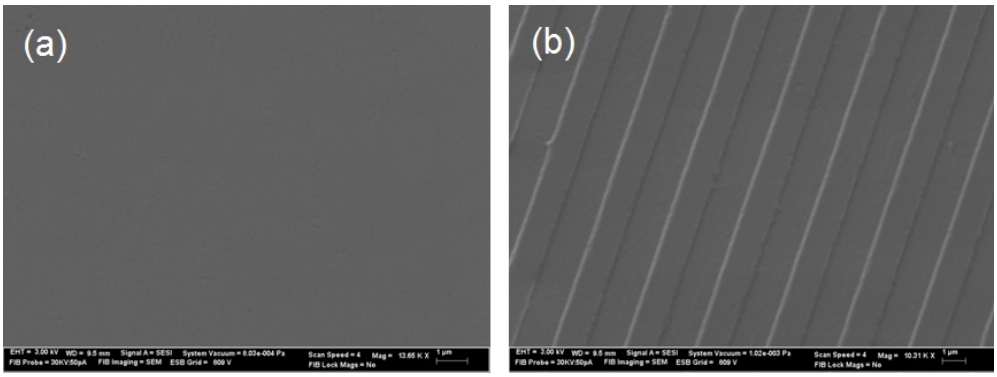

Figure 7. (a) SEM top-view of an $As_{20}Se_{80}$ film deposited on graphene; (b) ChG gratings on graphene patterned by thermal imprint.

As a simple proof-of-concept, we deposited $As_{20}Se_{80}$ ChG by single source thermal evaporation onto graphene grown by CVD on Ni substrates. SEM observation revealed a smooth, featureless glass film surface after deposition (Fig. 7a). Photonic structures were subsequently engraved into the glass layer using thermal nanoimprint. Fig. 7b shows a top-view SEM image of an optical grating in the $As_{20}Se_{80}$ layer patterned on graphene. Our Raman analysis further confirmed little structure change of the graphene prior to and after the glass photonic structure fabrication.

7. SUMMARY

The amorphous structure, low processing temperature, and large property tuning range of ChGs and transition metal oxides qualify them as the ideal material platform to enable substrate-blind photonic integration. Here we validated the unique substrate-blind integration capacity of these materials by demonstrating monolithic integration on fluoride crystals for mid-IR photonics, plastic substrate for flexible photonics, and graphene for emerging graphene-glass hybrid devices. We anticipate that the multi-material integration strategy can be extended to other technically important substrates including but not limited to functional oxides, metals, and ceramics to pave the path towards novel device applications.

This work was supported by the National Science Foundation under award number 1200406.

REFERENCES

[1] B. J. Eggleton, B. Luther-Davies, and K. Richardson, "Chalcogenide Photonics," Nat. Photonics 5, 141-148 (2011).
[2] N. Hô, M. Phillips, H. Qiao, P. Allen, K. Krishnaswami, B. Riley, T. Myers, and N. Anheier, "Single-mode low-loss chalcogenide glass waveguides for the mid-infrared," Opt. Lett. 31, 1860-1862 (2006).
[3] N. Carlie, J. D. Musgraves, B. Zdyrko, J. Hu, M. Torregiani, F. Morichetti, V. Singh, A. Agarwal, I. Luzinov, K. Richardson, L. C. Kimerling, and A. Melloni, "Integrated chalcogenide waveguide resonators for mid-IR sensing: Leveraging material properties to meet fabrication challenges," Opt. Express 18, 26728-26743 (2010).
[4] K. Richardson, L. Petit, N. Carlie, B. Zdyrko, I. Luzinov, J. Hu, A. Agarwal, L. C. Kimerling, T. Anderson, and M. Richardson, "Progress on the fabrication of on-chip, integrated chalcogenide glass (ChG)-based sensors," J. Nonlinear Opt. Phys. Mater. 19, 75-99 (2010).
[5] Y. Zha, M. Waldmann, and C. B. Arnold, "A review on solution processing of chalcogenide glasses for optical components," Opt. Mater. Express 3, 1259-1272 (2013).
[6] C. Tsay, Y. Zha, and C. B. Arnold, "Solution-processed chalcogenide glass for integrated single-mode mid-infrared waveguides," Opt. Express 18, 26744-26753 (2010).
[7] J. D. Musgraves, N. Carlie, J. Hu, L. Petit, A. Agarwal, K. Richardson, and L. C. Kimerling, "Comparison of the optical, thermal and structural properties of Ge-Sb-S thin films deposited using thermal evaporation and pulsed laser deposition techniques," Acta Mater. 59, 5032-5039 (2011).
[8] Y. Ruan, W. Li, R. Jarvis, N. Madsen, A. Rode, and B. Luther-Davies, "Fabrication and characterization of low loss rib chalcogenide waveguides made by dry etching", Opt. Express, 12, 5140-5145 (2004).
[9] A. Ganjoo, H. Jain, C. Yu, R. Song, J. Ryan, J. Irudayaraj, Y. Ding, and C. Pantano, "Planar chalcogenide glass waveguides for IR evanescent wave sensors", J. Non-Cryst. Sol., 352, 584-588 (2006).
[10] Y. Zha and C. B. Arnold, "Solution-processed 3D Chalcogenide Glass Waveguides," in CLEO:2011 - Laser Applications to Photonic Applications, OSA Technical Digest (CD) (Optical Society of America, 2011), paper JWA54.
[11] R. DeCorby, N. Ponnampalam, M. Pai, H. Nguyen, P. Dwivedi, T. Clement, C. Haugen, J. McMullin, S. Kasap, "High index contrast waveguides in chalcogenide glass and polymer", IEEE J. Sel. Top. Quant., 11, 539-546 (2005).
[12] Huang, C. C., D. Hewak, and J. Badding. "Deposition and characterization of germanium sulphide glass planar waveguides." Opt. Express 12, 2501-2506 (2004).
[13] Huang, C. C., K. Knight, and D. W. Hewak. "Antimony germanium sulphide amorphous thin films fabricated by chemical vapour deposition." Opt. Mater. 29, 1344-1347 (2007).
[14] Y. Zou, H. Lin, O. Ogbuu, L. Li, S. Danto, S. Novak, J. Novak, J. D. Musgraves, K. Richardson, and J. Hu, "Effect of annealing conditions on the physio-chemical properties of spin-coated As2Se3 chalcogenide glass films," Opt. Mater. Express 2, 1723-1732 (2012).
[15] J. Hu, N. Carlie, N. Feng, L. Petit, A. Agarwal, K. Richardson, and L. C. Kimerling, "Planar waveguide-coupled, high-index-contrast, high-Q resonators in chalcogenide glass for sensing," Opt. Lett. 33, 2500-2502 (2008).
[16] Y. Zou, L. Moreel, L. Savelli, H. Lin, J. Zhou, L. Li, S. Danto, J. D. Musgraves, K. Richardson, K. Dobson, R. Birkmire, and J. Hu, "Solution processing and resist-free nanoimprint fabrication of thin film chalcogenide glass devices: inorganic-organic hybrid photonic integration," Adv. Opt. Mater. 2, 759-764 (2014).
[17] Y. Zou, D. Zhang, H. Lin, L. Li, L. Moreel, J. Zhou, Q. Du, O. Ogbuu, S. Danto, J. D. Musgraves, K. Richardson, K. Dobson, R. Birkmire, and J. Hu, "High-Performance, High-Index-Contrast Chalcogenide Glass Photonics on Silicon and Unconventional Nonplanar Substrates," Adv. Opt. Mater. 2, 478-486 (2014).

[18] T. Han, S. Madden, D. Bulla, and B. Luther-Davies, "Low loss Chalcogenide glass waveguides by thermal nano-imprint lithography," Opt. Express 18, 19286-19291 (2010).
[19] H. Lin, L. Li, Y. Zou, S. Danto, J. D. Musgraves, K. Richardson, S. Kozacik, M. Murakowski, D. Prather, P. T. Lin, V. Singh, A. Agarwal, L. C. Kimerling, and J. Hu, "Demonstration of high-Q mid-infrared chalcogenide glass-on-silicon resonators," Opt. Lett. 38, 1470-1472 (2013).
[20] R. Sun, P. Dong, N. Feng, C. Hong, J. Michel, M. Lipson, and L. C. Kimerling, "Horizontal single and multiple slot waveguides: optical transmission at $\lambda = 1550$ nm," Opt. Express 15, 17967-17972 (2007).
[21] L. Zhang, Y. Yue, Y. Xiao-Li, J. Wang, R. G. Beausoleil, and A. E. Willner, "Flat and low dispersion in highly nonlinear slot waveguides," Opt. Express 18, 13187-13193 (2010).
[22] L. Li, H. Lin, S. Qiao, Y. Zou, S. Danto, K. Richardson, J. D. Musgraves, N. Lu, and J. Hu, "Integrated flexible chalcogenide glass photonic devices," Nat. Photonics 8, 643-649 (2014).
[23] J. Hu, L. Li, H. Lin, P. Zhang, W. Zhou, and Z. Ma, "Flexible integrated photonics: where materials, mechanics and optics meet," Opt. Mater. Express 3, 1313-1331 (2013).
[24] J. Park, S. Ozdemir, F. Monifi, T. Chadha, S. Huang, P. Biswas, and L. Yang. "Titanium Dioxide Whispering Gallery Microcavities." Adv. Opt. Mater. 2, 711-717 (2014).
[25] L. Colombo, R. Wallace, and R. Ruoff. "Graphene growth and device integration." Proc. IEEE 101, 1536-1556 (2013).